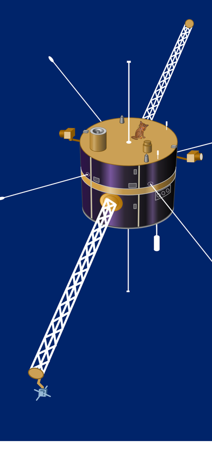

Gamma-ray Emission during Impulsive Phase of the 2017-Sep-06 X9.3 Flare

Alexandra L. Lysenko[1], Sergey A. Anfinogentov[2], Gregory D. Fleishman[3,1]

[1] Ioffe Institute, St. Petersburg, Russian Federation;
[2] Institute of Solar-Terrestrial Physics, Irkutsk, Russian Federation;
[3] New Jersey Institute of Technology, Center for Solar-Terrestrial Research, Newark, NJ, United States

Abstract

The minimum of solar cycle 24 demonstrated a series of strong flares that occurred in September, 2017, including four X-class flares. Two of them, the X9.3 flare on September, 6, and the X8.2 flare on September, 10, are of particular interest, because they were followed by a sustained gamma-ray emission observed by Fermi-LAT instrument during more than 10 hours at energies >100 MeV. While the second flare, X8.2, was well observed in microwave, HXR and gamma-ray ranges, observations of the impulsive phase of the first one, X9.3, are rather poor: the impulsive phase occurred during "nights" of both RHESSI and Fermi spacecraft.

Joint Russian-US experiment Konus-Wind, operating in the energy range 20 keV – 15 MeV and orbiting near Lagrange point L1, observed the impulsive phase of the 2017-Sep-06 X9.3 flare. The impulsive phase lasted from 11:54 to 12:03 UT and demonstrated a few peaks in HXR range and gamma-ray emission at energies up to a few MeV. We performed spectral analysis of this flare in HXR and gamma-ray ranges using the Bayesian statistics to distinguish between contributions from relativistic electron emission and emission in gamma-ray lines, for which accelerated ions are responsible. Bayesian inference revealed the presence of nuclear lines in the spectrum, thus ions were accelerated during 2017-Sep-06 X9.3 solar flare.

Table : Summary of the best Konus-Wind spectral fits in 200 keV–15 MeV energy range with best models

No.	t_{start} s	t_{stop} s	model	PL, γ	PL, A[a]	511 keV flux[b]	Nuclear line flux[b]	2.2 MeV flux[b]	CPL, γ	CPL, A[a]	CPL, E MeV	ln(P(D))	χ^2/dof	Prob.
0	11:56:03.6	11:57:17.1	PL+nuclear+2.2 MeV+CPL	$3.52^{+0.09}_{-0.08}$	$6.5^{+0.4}_{-0.4}$	…	$0.39^{+0.24}_{-0.24}$	$0.18^{+0.04}_{-0.04}$	$0.8^{+0.2}_{-0.4}$	$1.0^{+0.4}_{-0.4}$	$4.1^{+1.8}_{-1.6}$	-120.87	102.8/66	0.003
			PL+511 keV+nuclear+2.2 MeV+CPL	$3.58^{+0.09}_{-0.09}$	$6.3^{+0.4}_{-0.4}$	$0.07^{+0.04}_{-0.04}$	$0.41^{+0.25}_{-0.24}$	$0.18^{+0.04}_{-0.04}$	$0.8^{+0.2}_{-0.4}$	$1.1^{+0.4}_{-0.5}$	$3.8^{+1.7}_{-1.6}$	-121.66	93.2/65	0.01
1	11:56:03.6	11:56:11.5	PL+511 keV+nuclear+2.2 MeV+CPL	$3.68^{+0.22}_{-0.18}$	$7.0^{+0.8}_{-1.1}$	$0.09^{+0.10}_{-0.08}$	$0.82^{+0.51}_{-0.62}$	$0.09^{+0.10}_{-0.08}$	$0.6^{+0.4}_{-0.5}$	$0.61^{+0.94}_{-0.55}$	$3.3^{+2.1}_{-1.7}$	-175.87	57.7/65	0.73
2	11:56:11.5	11:56:19.7	PL+511 keV+nuclear+2.2 MeV+CPL	$3.39^{+0.13}_{-0.12}$	$8.4^{+0.5}_{-0.6}$	$0.08^{+0.10}_{-0.07}$	$0.86^{+0.35}_{-0.44}$	$0.23^{+0.12}_{-0.12}$	$0.6^{+0.4}_{-0.5}$	$0.12^{+0.58}_{-0.11}$	$9.7^{+4.9}_{-7.2}$	-187.64	83.3/65	0.06
3	11:56:19.7	11:56:27.9	PL+511 keV+nuclear+2.2 MeV+CPL	$3.40^{+0.16}_{-0.13}$	$10.2^{+0.9}_{-1.1}$	$0.09^{+0.10}_{-0.08}$	$0.70^{+0.51}_{-0.58}$	$0.16^{+0.12}_{-0.11}$	$0.6^{+0.3}_{-0.5}$	$0.52^{+0.99}_{-0.47}$	$3.9^{+1.6}_{-2.2}$	-189.54	77.7/65	0.14
4	11:56:27.9	11:56:36.1	PL+511 keV+nuclear+2.2 MeV+CPL	$3.34^{+0.11}_{-0.09}$	$18.1^{+0.9}_{-1.2}$	$0.13^{+0.13}_{-0.11}$	$1.12^{+0.54}_{-0.70}$	$0.23^{+0.13}_{-0.13}$	$0.6^{+0.4}_{-0.5}$	$0.46^{+1.09}_{-0.44}$	$5.3^{+6.0}_{-3.8}$	-188.51	63.5/65	0.53
5	11:56:36.1	11:56:44.3	PL+511 keV+nuclear+2.2 MeV+CPL	$3.27^{+0.17}_{-0.13}$	$9.4^{+0.7}_{-1.1}$	$0.09^{+0.10}_{-0.08}$	$1.12^{+0.44}_{-0.65}$	$0.34^{+0.13}_{-0.13}$	$0.6^{+0.4}_{-0.5}$	$0.32^{+1.04}_{-0.31}$	$5.4^{+5.9}_{-3.9}$	-190.64	81.6/65	0.08
6	11:56:44.3	11:56:52.5	PL+511 keV+nuclear+2.2 MeV+CPL	$3.61^{+0.44}_{-0.35}$	$3.1^{+0.8}_{-0.9}$	$0.05^{+0.07}_{-0.05}$	$0.24^{+0.32}_{-0.22}$	$0.33^{+0.12}_{-0.13}$	$0.8^{+0.2}_{-0.3}$	$1.01^{+0.80}_{-0.63}$	$3.1^{+1.2}_{-1.3}$	-172.89	59.0/65	0.18
7	11:56:52.5	11:57:00.7	PL+511 keV+nuclear+2.2 MeV+CPL	$3.75^{+0.99}_{-0.54}$	$1.6^{+0.6}_{-0.8}$	$0.08^{+0.12}_{-0.07}$	$0.38^{+0.45}_{-0.33}$	$0.16^{+0.11}_{-0.11}$	$0.7^{+0.3}_{-0.5}$	$0.87^{+0.44}_{-0.81}$	$2.7^{+1.2}_{-1.2}$	-175.28	76.6/65	0.15
8	11:57:00.7	11:57:08.9	PL+511 keV+nuclear+2.2 MeV+CPL	$3.88^{+0.39}_{-0.33}$	$1.8^{+0.4}_{-0.5}$	$0.08^{+0.08}_{-0.07}$	$0.66^{+0.27}_{-0.30}$	$0.20^{+0.11}_{-0.11}$	$0.5^{+0.4}_{-0.5}$	$0.05^{+0.40}_{-0.05}$	$11.3^{+3.5}_{-8.7}$	-174.90	85.3/65	0.05
9	11:57:08.9	11:57:17.1	PL+511 keV+nuclear+2.2 MeV+CPL	$4.22^{+0.52}_{-0.46}$	$1.7^{+0.6}_{-0.6}$	$0.10^{+0.08}_{-0.08}$	$0.46^{+0.44}_{-0.40}$	$0.10^{+0.10}_{-0.09}$	$0.7^{+0.3}_{-0.5}$	$0.45^{+0.53}_{-0.42}$	$6.0^{+6.7}_{-4.5}$	-178.02	79.1/65	0.11

[a] In units of 10^{-3} photons cm^{-2} s^{-1} keV^{-1} at 500 keV.

[b] In units of photons cm^{-2} s^{-1}.

Konus-Wind Instrument

- Konus-Wind consists of two 13 cm x 7.5 cm NaI(Tl), which are located on opposite faces of the Wind spacecraft, observing the southern and the northern ecliptical hemispheres.
- Konus-Wind operating modes
  - Waiting mode:
    Count rate in 3 energy channels: G1 (∼20–80 keV), G2 (∼80–300 keV), G3 (∼300–1200 keV) with accumulation time 2.944 s.
  - Triggered mode:
    - Count rate in 3 channels with variable time resolution from 2 to 256 ms, the total duration ∼240 s.
    - 64 multichannel spectra in two partially overlapping energy ranges ∼20 keV–15 MeV. Accumulation times: 64 ms–8.192 s.
- After accumulation of energy spectra the instrument is inactive for ∼1 hour, when the count rate is available only in G2 channel with accumulation time 3.6 s.
- All the data for solar flares registered by Konus-Wind instrument in the triggered mode are available on-line at http://www.ioffe.ru/LEA/kwsun.
- Detailed instrument description can be found in Aptekar et al. [1995].

Observation

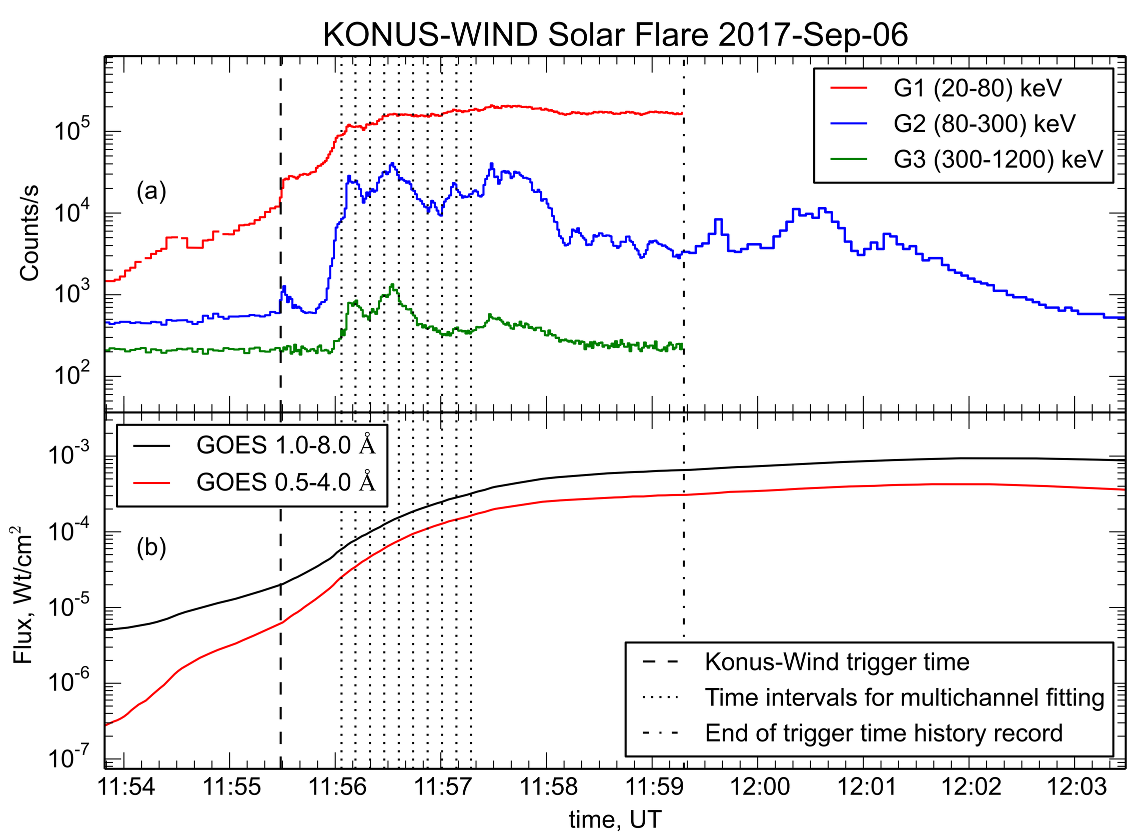

- Konus-Wind observed 2017-Sep-06 X9.3 flare in the triggered mode since 11:55:29.0 UT.
- Time history in G1, G2, G3 channels with high temporal resolution is available since 11:55:29.0 UT till 11:59:18.7 UT.
- Multichannel energy spectra in two partially overlapping energy ranges are available from 11:55:29.0 UT to 11:57:17.1 UT.
- Multichannel spectral fitting in 200 keV–15 MeV energy range was held on nine time intervals, where gamma-ray emission (≳500 keV) was observed.
- After the end of the trigger record 3 more maxima in G2 channel are observed, but, unfortunately, there are no other measurements for this period.

Acknowledgements

This work was supported by RFBR grant 18-32-00439.

On-line material

PDF version of this poster is available on-line via http://www.ioffe.ru/LEA/SF_AR/gallery.html.

Gamma-ray spectrum

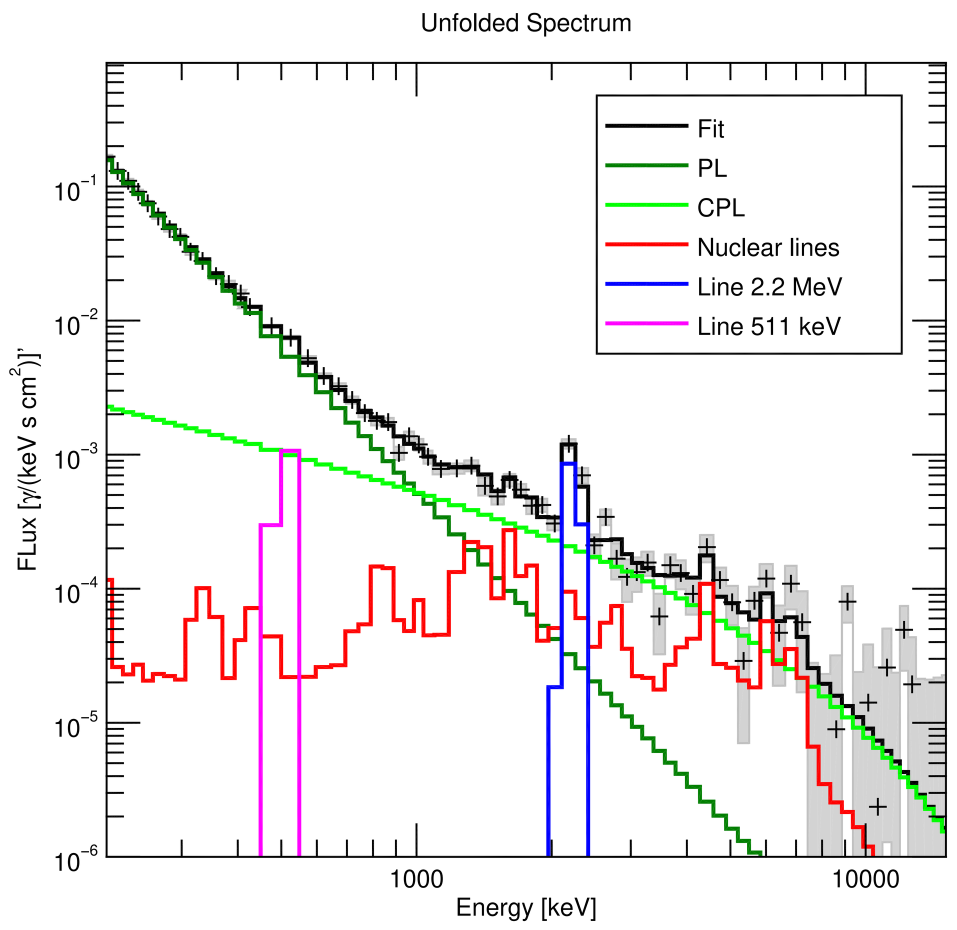

Gamma-ray emission in solar flares could be formed by:

- Bremsstrahlung continuum from accelerated electrons and positrons (fitted by power law PL, broken power law, power law with exponential cutoff at higher energies CPL).
- Nuclear deexcitation lines (fitted by, for example, $nuclear$ template from Murphy et al. [2009]).
- Electron-positron annihilation line at 511 keV (fitted by gaussian line).
- Neutron capture line (n + p → d) at 2.2 MeV (fitted by very narrow gaussian line).
- Contunuum from pion decay observed at tens of MeV energies – outside Konus-Wind spectral range.

Questions:

- How close is the best fit to the actual observations?
- What model is better confined in the parameter space (has narrower uncertainties)?
- What model is better confined in the observational data space (predicts possible observations closer to the actual data)?
- What model components (PL, CPL, nuclear lines, etc.) actually present in the flare spectrum?

Bayesian inference gives the answer by calculating the $Bayes Factor$.

Bayesian inference

- Bayesian inference implies investigation of the Posterior probability distribution function (PDF) which can be calculated using the Bayes theorem:

$$P(\theta|D) = \frac{P(D|\theta)P(\theta)}{P(D)}, \quad (1)$$

where $\theta = \theta_i$ is the model parameter set, $P(\theta)$ is their prior distribution, and $P(D|\theta)$ is the likelihood function. The normalisation constant $P(D)$ is the Bayesian Evidence or marginalised likelihood:

$$P(D) = \int P(D|\theta)P(\theta)d\theta. \quad (2)$$

- Two competing models M_1 and M_2 can be quantitatively compared by computing the Bayes Factor:

$$B_{12} = \frac{P(D|M_1)}{P(D|M_2)}, \quad (3)$$

$1 \leq B_{12} \leq 3$ - preferable model can't be found out, $3 \leq B_{12} \leq 20$ – positive evidence in favour of model M_1, $B_{12} > 20$ – strong evidence in favour of model M_1.

- To sample posterior distribution, we use Markov Chain Monte-Carlo (MCMC) technique. The sampling code is our own implementation of the Metropolis-Hastings algorithm [Pascoe et al., 2017].

Spectral analysis results

- To establish the presence of different spectral components in the observed HXR spectra, we analyzed integral spectrum with different component combinations: $PL + 511\,keV + nuclear + 2.2\,MeV + CPL$, $PL + CPL$, $PL + nuclear + 511\,keV + 2.2\,MeV$, etc., and calculated the appropriate Bayes factors.
- We got strong evidence in favour of nuclear deexcitation lines, flatter CPL continuum in MeV range and neutron capture line at 2.2 MeV in gamma-ray spectrum, and possible presence of e+-e- annihilation line at 511 keV (see the Table), which implies that the flare was accompanied by ion acceleration.
- We analyzed multichannels spectra during nine time intervals with the following model combinations: $PL + 511\,keV + nuclear + 2.2\,MeV + CPL$. Obtained model parameters are presented in the Table and in the Figure.
- To estimate the flare flux and spectral evolution in HXR range with high temporal resolution and during longer period, than multichannel data allows, and to compare results with gamma-ray range we fitted two channels G2 and G3 with simple power law model (degrees of freedom=0) for time period where background excess in G3 channel was observed on 2.048 s time bins.

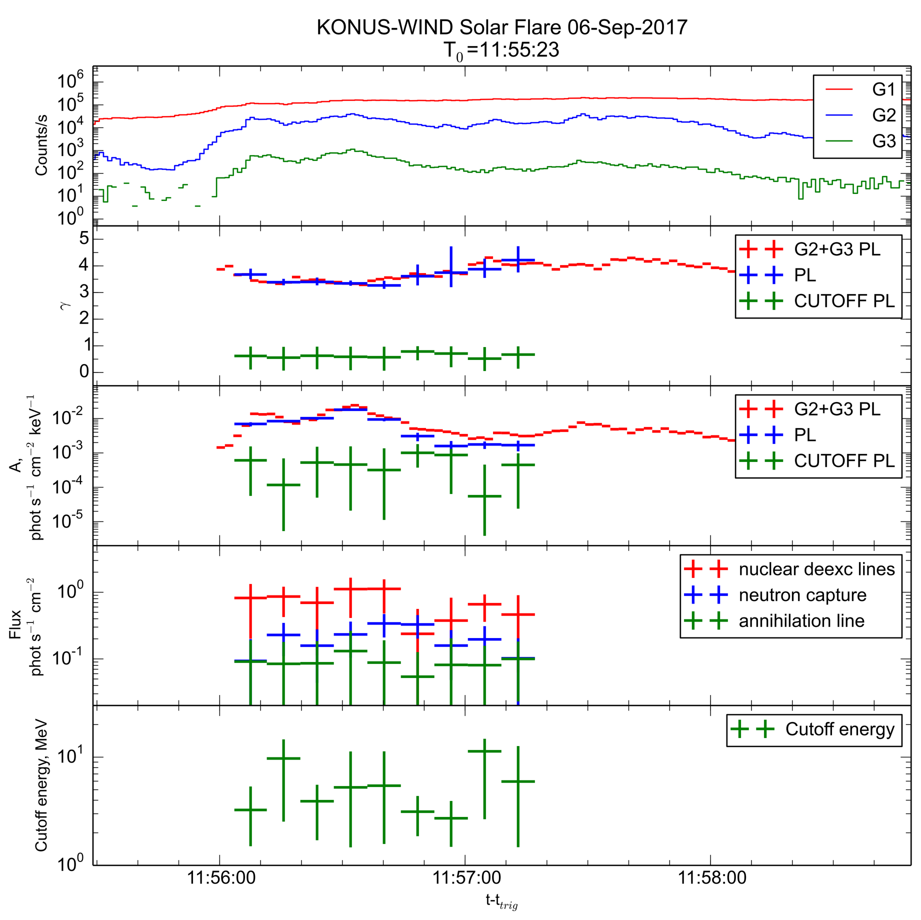

- Bremsstrahlung continuum in lower energy range (PL model) demonstrates soft-hard-soft spectral evolution during the main flare peaks.
- Proton spectral index in ≲30 MeV energy range is s=$3.5^{+1.5}_{-1.0}$ as estimated through the neutron capture flux to nuclear deexcitation lines flux ratio [Hua & Lingenfelter, 1987].
- Flatter CPL component of the continuum could be caused by relativistic electrons and positrons produced in nuclear reactions.

Conclusions

- 2017-Sep-06 X9.3 flare demonstrated gamma-ray emission up to ∼10 MeV.
- Bayesian analysis confirmed the presence of nuclear deexcitation lines and neutron capture line at 2.2 MeV. We did not find strong evidence in favor of the electron-positron annihilation line at 511 keV, but its presence cannot be excluded.
- Bayesian analysis confirmed the presence of additional continuum component described by power law with exponential cutoff at higher energies.
- 2017-Sep-06 X9.3 flare efficiently accelerated ions as evidenced by the presence of nuclear deexcitation lines and neutron capture line in gamma-ray spectrum.

References

Aptekar R. L. et al. Konus-W Gamma-Ray Burst Experiment for the GGS Wind Spacecraft Space Sci. Rev. 71, 1, 265 (1995)

Murphy, R. J. Kozlovsky, B. Kiener, J. Share, G. H. Nuclear Gamma-Ray De-Excitation Lines and Continuum from Accelerated-Particle Interactions in Solar Flares ApJS. 183, 1, 142 (2009)

Hua, X. M. Lingenfelter, R. E. Solar flare neutron production and the angular dependence of the capture gamma-ray emission SoPh. 107, 2, 351 (1987)

Pascoe, D. J. Anfinogentov, S. Nisticò, G. Goddard, C. R. Nakariakov, V. M. Coronal loop seismology using damping of standing kink oscillations by mode coupling: II. additional physical effects and Bayesian analysis A&A. 600, id.A78, 22 pp.(2017)

alexandra.lysenko@mail.ioffe.ru